Electronic excitation of gas-phase furan molecules by electron impact

Romarly F. da Costa*
Centro de Ciências Naturais e Humanas, Universidade Federal do ABC, 09210-170, Santo André, SP, Brazil

Márcio H. F. Bettega
Departamento de Física, Universidade Federal do Paraná, Caixa Postal 19044, 81531-990, Curitiba, Paraná, Brazil

Marco A. P. Lima
Laboratório Nacional de Ciência e Tecnologia do Bioetanol, Centro Nacional de Pesquisa em Energia e Materiais, Caixa Postal 6170, 13083-970, Campinas, SP, Brazil
Instituto de Física Gleb Wataghin, Universidade Estadual de Campinas, Caixa Postal 6165, 13083-970, Campinas, SP, Brazil

Maria C. A. Lopes
Departamento de Física, ICE, Universidade Federal de Juiz de Fora, 36036-330, Juiz de Fora, MG, Brazil

Leigh R. Hargreaves, Gabriela Serna, and Murtadha A. Khakoo
Department of Physics, California State University, Fullerton, California 92834, USA
(Received 3 April 2012; published 25 June 2012)

Experiments and *ab initio* calculations of the differential and integral cross sections for the electronic excitation from the ground state $^1A_1$ to the $^3B_2$ and $^3A_1$ states of gas-phase furan molecules by low-energy electron impact were performed. Experimental differential cross sections were measured at incident electron energies between 5 and 15 eV and for scattering angles from 10° to 130°. The calculated cross sections were obtained using the Schwinger multichannel method implemented with pseudopotentials. The influence of channel-coupling and polarization effects is investigated through the comparison between three different models of scattering calculations, each one considering a distinct channel-coupling scheme. The comparison of experimental and calculated cross sections for electronically inelastic electron scattering by C_4H_4O molecules is found to be mostly reasonable. The existing discrepancies in this combined theoretical and experimental study help to illustrate difficulties in readily establishing reliable electronic excitation cross sections of polyatomic molecules by low-energy electrons.

DOI: 10.1103/PhysRevA.85.062706 PACS number(s): 34.80.Gs, 34.80.Bm

I. INTRODUCTION

Electron-induced breakage of chemical bonds through dissociative electron attachment, a process mediated by the formation of temporary anionic states, has been recognized as a very efficient mechanism leading to the production of permanent lesions on DNA chains in the form of single- and double-strand breaks [1–5]. Much of the latest ongoing work on this subject has been devoted to the study of inelastic processes, more specifically, those involving electronic and/or vibrational excitations of the DNA basic constituents by impact of low-energy electrons [6–11]. In particular, the electronic excitation cross sections obtained in these studies revealed the presence of several core-excited resonances that appear at energies ranging typically from 5 to 10 eV. These findings are relevant because the formation of such short-lived negative-ion states represents an alternative, and probably rather effective if compared to "one-particle" shape resonances, doorway for electron-induced damage to DNA. Thus, the determination of electronic excitation cross sections for biomolecules (such as the nitrogenous bases or the phosphate group) certainly represents a crucial step towards a deeper insight into the mechanisms of DNA damage by secondary electrons and establishes itself as a challenging task for experimentalists and theoreticians. From the experimental point of view, the difficulties for obtaining reliable cross sections are related to the resolution of the molecular spectra via energy-loss assignments and widths of spectral features observed and also to the sensitivity of handling very low energy electrons in the electron spectrometer. From the theoretical perspective, there are also subtle aspects related to the description of such kinds of processes, observed in applications involving relatively small molecules with low-lying excited states, which should be considered so as to assess their influence on larger systems that also exhibit this specific characteristic.

Recent investigations concerning electron collisions with furan [12] and ethylene [13,14] molecules demonstrated the importance of including polarization effects for an accurate description of the electronic excitation process. A particular feature that these two molecules have in common is the presence of a first excited triplet state lying at energies around 4 eV (see, for instance, Ref. [15]). As is well known, taking the polarization of the target into account in the scattering calculations is very important for describing the elastic process at the low-energy range, especially with regard to the position of the resonances [16]. The results obtained in Refs. [12–14] indicated that the inclusion of these effects also has a strong influence on the electronic excitation process, leading to a

*romarly.costa@ufabc.edu.br

significant change in the magnitude of the inelastic cross sections. In summary, these theoretical studies suggest that for molecular systems supporting resonances near low-energy electronic thresholds, standard close-coupling calculations may produce inaccurate results because of the lack of proper treatment of the polarization effects, which will give rise to misplaced resonances in the elastic coupled channel. For the $X^1A_g \rightarrow \tilde{a}^3B_{1u}$ transition in ethylene, the differential cross sections (DCSs) obtained at the two-channel close-coupling–plus–polarization level of approximation are in much better agreement with the experimental data compared to those obtained within scattering calculations where only channel-coupling effects were considered, as reported in [13,14]. The two studies on electronic excitation of C_2H_4 by electron impact mentioned above have clarified the origin of the discrepancies between theoretical and experimental results observed for that system, which had remained without a satisfactory explanation for many years. In the case of furan, to our knowledge, there are no reported measurements or calculations with which to compare our electronically inelastic cross sections.

However, it is worth noting that a careful review of the literature on the subject shows that, with the exception of electronic excitation, the number of studies related to electron collisions with furan is appreciable and has increased significantly in recent years. Early experimental works performed by van Veen [17] and by Flicker *et al.* [18,19] are mainly concerned with the characterization of the electron-impact excitation spectra of furan, thiophene, and pyrrole molecules by means of angle-differential energy-loss spectroscopic measurements. Dissociative electron attachment to a series of five-membered heterocyclic compounds were investigated by Muftakhov and coworkers [20]. Using the mass spectroscopy technique, these authors identified a number of structures which, for furan, appeared in the energy range from 3.5 to 10.7 eV and were assigned as core-excited Feshbach resonances having as parent states the first triplet excited state and a series of singlet excited states. Evidence of two negative-ion resonances centered at around 1.8 and 3.1 eV, first reported by Modelli and Burrow [21], is in very good agreement with the assignments observed in elastic calculations carried out by Bettega and Lima [22], in a joint experimental-theoretical effort on elastic electron scattering conducted by Khakoo *et al.* [23], and, more recently, in the total-cross-section measurements performed by Szmytkowski *et al.* [24]. A broader structure having its maximum at about 8 eV was also reported in Refs. [22–24], but no attempts to ascribe it to a more specific mechanism of electron capture was provided by these authors. Studies on resonant dissociative electron attachment to furan performed by Sulzer *et al.* [25] showed that during the resonant process several anionic fragments are formed. In particular, the results obtained in that work pointed out the existence of a core-excited shape resonance centered at 6 eV, which was also observed in the electron-energy-loss measurements done by Motte-Tollet *et al.* [26]. More recently, using the electron-impact optical excitation technique, Dampc and Zubek [27] studied the production of excited fragments in furan. Dissociation and fragmentation processes considered in this work lead to the formation of a number of electronically excited atomic as well as molecular fragments in the energy range between 15 and 95 eV. Finally, experimental differential cross sections for vibrational excitation structures in the electron-energy-loss spectra of furan in the range of 0 to 0.8 eV were also determined at incident energy (E_0) values of 5.0, 6.0, 7.5, 9.0, 10.0, and 15.0 eV and scattering angles (θ) in the range of 10° to 130° by Hargreaves *et al.* [28]. The measurements performed by these authors revealed the presence of a broad resonant feature at an E_0 value of about 7.5 eV for most of the vibrational energy-loss features. This was consistent with the results obtained in Ref. [26].

Motivated by the growing interest in studies of electronic excitation of molecules by electron impact and also by the need for electron collision data for furan through which we could compare and relate our results, we decided to return to this matter and execute a series of measurements and *ab initio* calculations for the electronic excitation of furan by low-energy electron impact. In this paper, we focus on the electron-impact excitation of the $^1A_1 \rightarrow {}^3B_2$ and $^1A_1 \rightarrow {}^3A_1$ electronic transitions and will also discuss the present theory as it pertains to an improvement compared to a previous model applied to elastic scattering. Here, *ab initio* calculations were performed using the Schwinger multichannel method (SMC) [29] implemented with pseudopotentials (SMCPP) [30]. Elastic calculations were performed at the static-exchange and static-exchange–plus–polarization levels of approximation, while electronic inelastic calculations were carried out at different levels (up to nine) of channel coupling, with and without the inclusion of polarization effects.

The organization of the paper is as follows. In Secs. II and III we describe the experimental setup with details of the furan excitation experiment. In Secs. IV and V theoretical aspects of the SMC method are briefly reviewed, and we present a summary of the computational details relative to the description of furan target and to the scattering calculations. Thereafter, experimental and theoretical results obtained in this work are presented and discussed, and in the final section, we summarize our findings with some conclusions.

II. EXPERIMENTAL SETUP

The experimental apparatus has been described in previous articles, e.g., by Khakoo *et al.* [31], and so only a brief description will be given here. The electron gun and the detector employed titanium double-hemispherical energy selectors and cylindrical lenses (also titanium), equipped with molybdenum apertures, used to transport, focus, and collimate electrons emitted from a thoriated tungsten cathode onto a gas jet of furan molecules. The spectrometer system was baked to about 130 °C by magnetically free biaxial heaters (ARi Industries model BXX06B41-4K). The analyzer's detector was a discrete dynode electron multiplier (Equipe Thermodynamique et Plasmas model AF151) with a background rate less than 0.01 Hz and a uniform detection efficiency for electron count rates up to 1 MHz. The remnant magnetic field in the collision region was reduced to around 1 mG by using a double μ-metal shield as well as a coil that reduced the vertical component of the earth's magnetic field.

Typical electron currents at the collision region were around 30 nA at all energies reported in this study. The electron-beam current varied by less than 5% over the course

of several days, subject to minor periodic retuning of the spectrometer to maintain the long-term stability. The energy of the beam E_0 was established by determining the cutoff in the energy-loss spectrum at zero residual energy. Alternatively, the beam energy could be calibrated against the dip in the He elastic-scattering cross section due to the $2\,^2S$ He resonance at 19.366 eV [32]. Both methods gave good agreement with each other regarding the determination of E_0. Typically, the contact potential, so determined, stayed between 800 and 900 meV, with an uncertainty of 40 meV, over the multiweek course of the experiments. The energy resolution of the electron beam was approximately 70 meV.

Energy-loss spectra of the elastic peak were collected at fixed E_0 values and θ by repetitive multichannel-scaling techniques. The angular resolution of the electron analyzer was 2°, full width at half maximum. The effusive target gas beam was formed by flowing gas through a thin aperture source 0.3 mm in diameter that was described previously [33]. This source was covered with carbon soot, using a pure acetylene flame, to reduce secondary electrons and placed 6 mm below the axis of the electron beam, incorporated into a movable source arrangement [34]. The movable gas source method determines background scattering rates expediently and accurately. The vapor pressure behind the source for furan was about 0.3 to 0.4 Torr, and the pressure in the experimental chamber was $\sim 4 \times 10^{-6}$ Torr. The operation of the experiment was entirely automated; the data-acquisition computer controlled the angular positioning of the spectrometer, monitored the target gas drive pressure, modulated the gas beam, and acquired the energy-loss spectra. The gas-beam temperature, determined by the apparatus temperature in the collision region, was about 130 °C; however, in most of the gas-handling copper tubing, the temperature was 24 °C. The higher temperature was in the last 4 cm of the gas-handling system before the gas exited into the collision region. Furan vapor was obtained from stabilized liquid furan (>99.0% purity), which was degassed using multiple freeze-pump-thaw cycles.

III. EXPERIMENTAL DETAILS

Electron-energy-loss spectra (EELS) were taken at E_0 values of 5, 6, 7.5, 10, and 15 eV and for θ ranging from 10° to 130°. The spectrometer's transmission efficiency at different residual electron energies was determined by measuring EELS for nitrogen and then normalizing ratios of the inelastic to elastic peaks against those reported by Le Clair and Trajmar [35], who employed a time-of-flight energy analyzer which was essentially free of residual electron-energy-transmission effects. For this work, we used the data of Le Clair and Trajmar, which covered all the valence bands below the C $^3\Pi_u$ state for E_0 values as low as 7.5 eV (their region I) as well as the C $^3\Pi_u$ bands (their region II) as a check. To determine the transmission efficiencies at $E_0 \leqslant 7.5$ eV, helium EELS were record at $E_0 = 34$ eV and $\theta = 90°$. The measured helium data were compared with the well-established inelastic differential cross sections from convergent close-coupling calculations by Fursa and Bray [36]. The transmission efficiencies were then determined using inelastic to inelastic ratios. For the helium ionization continuum the results of Schow *et al.* [37] were employed using the fact that the ionization continuum is flat at this particular E_0 and θ. An example of a furan EELS recorded in this work is shown in Fig. 1, taken at an incident energy of 10 eV and scattering angle of 40°. The lowest-lying $^3B_2$ and $^3A_1$ states are easily observed, as well as several higher-lying states, most of which are only partially resolved.

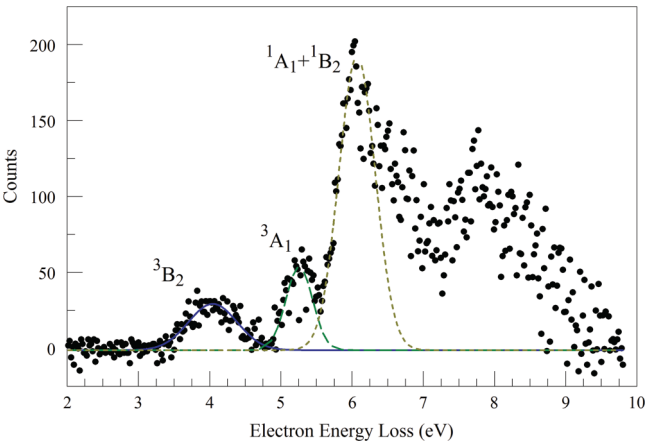

FIG. 1. (Color online) Background-subtracted electron-energy-loss spectrum of furan at the higher E_0 of 10.0 eV and $\theta = 40°$. The dashed lines are Gaussian fits used to unfold the individual electronic states (labeled).

As can be seen from Fig. 1, the $^3B_2$ state is largely separated, but the $^3A_1$ state is fractionally overlapped with higher-lying states. To unfold the spectrum, Gaussian peaks were fitted at the energy locations of the $^3B_2$ (3.97 eV) and $^3A_1$ (5.15 eV) states as reported by Guiliani and Hubin-Franskin [38]. A third peak was also fitted at approximately 6.0 eV to represent the contribution of the $^1A_1 + {}^1B_2$ higher-energy-loss state in order to separate this contribution from the $^3A_1$ state. Higher-lying states than $^1A_1 + {}^1B_2$ were not fitted for the present study. The fitting of the EEL spectrum was performed using an open-source data analysis and plotting software package (QTIPLOT [39]). Once fitted the areas under the $^3B_2$ and $^3A_1$ peaks were compared with the area under the elastic peak (also fitted with a single Gaussian profile to remove any contribution from vibrationally inelastic scattering) and the measured elastic cross sections of Khakoo *et al.* [23] and corrected for spectrometer transmission using the method described above to determine the final DCSs values.

IV. THEORY

Although the SMC and SMCPP methods have been described in detail elsewhere [29,30], we will present a summary of some details which are relevant for the discussion that follows. In the SMC method the resulting variational expression for the scattering amplitude in the body reference frame can be written as

$$f(\vec{k}_i,\vec{k}_f) = -\frac{1}{2\pi}\sum_{m,n}\langle S_{\vec{k}_f}|V|\chi_m\rangle (d^{-1})_{mn}\langle\chi_n|V|S_{\vec{k}_i}\rangle, \quad (1)$$

where the d_{mn} matrix elements are given by

$$d_{mn} = \langle\chi_m|A^{(+)}|\chi_n\rangle \quad (2)$$

and the $A^{(+)}$ operator is given by

$$A^{(+)} = \frac{1}{2}(PV + VP) - VG_P^{(+)}V + \frac{\hat{H}}{N+1} - \frac{1}{2}(\hat{H}P + P\hat{H}). \quad (3)$$

In Eqs. (1)–(3) the χ_m's, also known as configuration-state functions (CSFs), are $(N+1)$-electron Slater determinants constructed from products of target states with one-particle wave functions:

$$\{|\chi_m\rangle\} = \{|\chi_{ij}\rangle\} = \mathcal{A}_{N+1}[|\Phi_i(1,\ldots,N)\rangle \otimes |\varphi_j(N+1)\rangle], \quad (4)$$

where $|\Phi_i\rangle$ are N-electron Slater determinants obtained by single excitations from the occupied (hole) orbitals to a set of unoccupied (particle) orbitals. As before, $|\varphi_j\rangle$ is represented by a one-electron wave function, and $\mathcal{A}_{N+1}$ is the antisymmetrizing operator which accounts for the projectile electron's indistinguishability from the target electrons. From these products, only overall doublet states are retained if the target is a closed-shell system, as discussed in Ref. [40]. $S_{\vec{k}_{i(f)}}$ is an eigenstate of the unperturbed Hamiltonian H_0, given by the product of a target state and a plane wave with momentum $\vec{k}_{i(f)}$; V is the interaction potential between the incident electron and the target. $\hat{H} \equiv E - H$ is the total energy of the collision minus the full Hamiltonian of the system, with $H = H_0 + V$. P is a projection operator onto the open-channel electronic space of the target,

$$P = \sum_{l \in \text{open}} |\Phi_l\rangle\langle\Phi_l|, \quad (5)$$

and $G_P^{(+)}$ is the free-particle Green's function projected on the P space. In our applications of the SMCPP method we have been using the norm-conserving pseudopotentials of Ref. [41] in order to represent the inner electrons close to the nuclei, as described in Ref. [30].

The analysis for numerical stability of the present calculations is performed through a check procedure originally developed to investigate the origin of unphysical resonances appearing in positron-N_2 calculations [42]. Adapted to the case of electron-molecule scattering [40], the analysis begins with the diagonalization of the matrix elements of the $\tilde{V}$ operator:

$$\tilde{V} \equiv \frac{1}{2}(PV + VP) + \frac{\bar{H}}{N+1} - \frac{1}{2}\left(\bar{H}P + P\bar{H}\right), \quad (6)$$

where V and P have already been defined and $\bar{H} = \hat{H}$, calculated at a fixed energy. A next step consists of the identification and removal of the configurations weakly coupled by this average potential, that is, the eigenvectors associated with the eigenvalues near zero of the equation $\tilde{V} \mid \tilde{\chi}_m\rangle = v_m \mid \tilde{\chi}_m\rangle$. The $\tilde{\chi}_m$'s are then used as a new $(N+1)$-electron basis functions.

V. COMPUTATIONAL DETAILS

Before starting the description of the technical aspects related to the computational procedures used to calculate the scattering amplitudes of interest for this study, we believe it is important to highlight some general aspects that contributed in defining the level of approximation through which present calculations were performed. As is well known, the theoretical modeling of electron collisions with molecules is a very complex task, and in order to get an appropriate description of this process we need to have a good balance between several aspects, such as (i) a suitable choice of basis set functions to be used in the expansion of bound and excited target states and continuum scattering orbitals, (ii) an adequate treatment of polarization effects, which account for the distortion of the target's electronic cloud due to the presence of the incident electron and which are very important at low impact energies, and (iii) the inclusion of multichannel coupling effects describing the competition among all states that become energetically accessible to the target during the collision. Due to computational limitations, the use of approximations is necessary, and specific choices related to each one of the aspects mentioned above (such as the number of basis set functions, the amount of polarization, the number of coupled channels, etc.) need to be made so as to maintain the compromise between a sufficiently complete description of the problem in question and the ability to carry out the computational calculations.

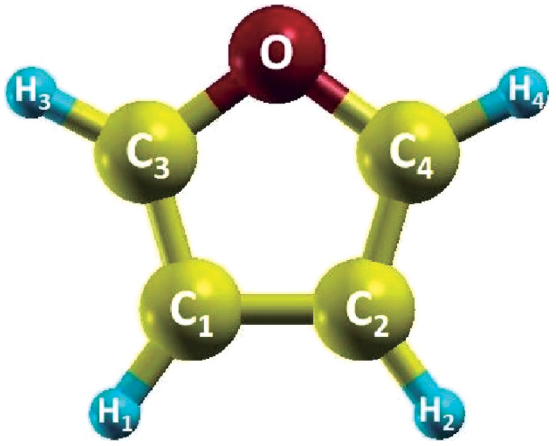

FIG. 2. (Color online) Ball and stick model structure of furan (C_4H_4O) obtained with the XCRYSDEN software [53].

In the present work, three different models were used to study the electronic excitation of furan by electron impact. In all these models, the ground state was computed in the Hartree-Fock approximation. Bound-state and scattering calculations were performed within the C_{2v} point group at the experimental equilibrium geometry [43] defined by the bond lengths R(O-C_3) = R(O-C_4) = 1.362 Å, R(C_1-C_2) = 1.434 Å, R(C_1-C_3) = R(C_2-C_4) = 1.361 Å, and R(C_1-H_1) = R(C_2-H_2) = R(C_3-H_3) = R(C_4–H_4) = 1.076 Å and by the angles θ(C_3-O-C_4) = 106.6°, θ(O-C_3-H_3) = θ(O-C_4-H_4) = 115.9°, and θ(C_3-C_1-H_1) = θ(C_4-C_2-H_2) = 127.9°. Furan is a planar molecule in its electronic ground state and presents a twofold axis of rotation that contains the oxygen atom and two vertical planes of symmetry (Fig. 2), leading, as a result, to four irreducible representations, labeled as A_1, A_2, B_1, and B_2 symmetries. The basis set employed within the Hartree-Fock approximation in our study was the same as the one used in the calculations presented in our previous joint experimental-theoretical work on elastic electron scattering from furan [23] and consists of square-integrable functions generated

TABLE I. Energy thresholds of the states composing the space of coupled channels.

		Energy (eV)							
	1 channel	2 channels	3 channels	4 channels	5 channels	6 channels	7 channels	8 channels	9 channels
Model 1	Elastic	3.68	5.12	7.72	7.74	8.39	8.55	10.97	11.03
Model 2	Elastic	3.66	7.20	8.47	8.87	9.76	10.93	14.89	15.53
Model 3	Elastic	5.10	7.64	8.36	11.01	14.90	16.14	17.63	18.08

by a variational method [44]. For carbon atoms the basis set is composed of $5s5p2d$ uncontracted Cartesian-Gaussian (CG) functions with exponents 12.49628, 2.470286, 0.614028, 0.184028, and 0.039982 for the s–type functions; 5.228869, 1.592058, 0.568612, 0.210326, and 0.072250 for the p-type functions; and 0.603592 and 0.156753 for the d-type functions. Oxygen atoms are described by a $5s5p2d$ set of uncontracted CG functions with exponents 16.05878, 5.920242, 1.034907, 0.316843, and 0.065203 for the s-type functions; 10.14127, 2.783023, 0.841010, 0.232940, and 0.052211 for the p-type functions; and 0.756793 and 0.180759 for the d-type functions. For hydrogen atoms we used the $4s$ (contracted to $3s$) basis set of Dunning [45]. The dipole moment obtained with this basis set was 0.85 D, which is in reasonable agreement with the experimental value of 0.66 D.

With regard to the description of multichannel coupling effects, in the three models considered here, the scattering calculations were performed at a nine-state close-coupling level of approximation, and the states used in the composition of the space of coupled channels, as well as their corresponding threshold energies, were obtained according to the minimal orbital basis for a single-excitation configuration interaction (MOB-SCI) strategy [40]. The main purpose in using this strategy was to provide a good description of the first few excited states of the target in terms of the SCI technique while keeping the size of the associated pseudostate space as small as possible. As discussed before, the idea behind the use of this procedure was based on the fact that an excited state constructed from an improved virtual orbital (IVO) [46] and calculated for a specific hole orbital is equivalent to a complete single-excitation configuration interaction (SCI) calculation out of the same hole orbital that generates the IVO. In the case of furan, as will be explained below, it is not completely equivalent because in describing the excited states of interest to the present study it was necessary to use IVOs coming from two distinct occupied orbitals. In practice, the implementation of the MOB-SCI strategy used in the present study was undertaken as follows. By running a full SCI calculation we found that the description of the $^3B_2$ state was mainly due to contributions of hole-particle transitions of the types $b_1 \rightarrow a_2$ and $a_2 \rightarrow b_1$. Similarly, in describing the $^3A_1$ state we observed that contributions from hole-particle transitions of the types $b_1 \rightarrow b_1$ and $a_2 \rightarrow a_2$ were strongly coupled to each other. Now, aiming to investigate the influence of different multichannel coupling schemes on the cross-section results for the electron-impact electronic excitation from ground state to the $^3B_2$ and $^3A_1$ states of the furan molecule, we used three different models described in detail in the following. One of these models, hereafter referred to as model 1, was constructed in order to include both transitions; i.e., the $^1A_1 \rightarrow {}^3B_2$ and the $^1A_1 \rightarrow {}^3A_1$ excitations are considered in the same round of calculations and compete among themselves (and, of course, with excitations to the other states present in the space of coupled channels, as listed in the first row of Table I) for the flux that defines the cross sections. In this case, the active space for the SCI calculation was composed by two holes (the b_1 and a_2 highest occupied orbitals) and two particles (a triplet IVO of the b_1 symmetry and a triplet IVO of the a_2 symmetry). Orbitals comprising the particle subspace were orthogonalized among themselves and with respect to all remaining IVOs through the usual Gram-Schmidt procedure. As a result we obtained two 4×4 matrices (eigenvectors and eigenvalues) for the overall $^2B_2$ and $^2A_1$ symmetries, one for the triplet and another for the singlet Hamiltonians. By diagonalizing these matrices it was possible to provide a good description of the two low-lying triplet states ($^3B_2$ and $^3A_1$) of the target at the same time. Each of the other two models, in turn, include the excitation to only one of the excited states of interest: the $^1A_1 \rightarrow {}^3B_2$ transition is

TABLE II. Comparison of the excitation energies for furan, as obtained from several theoretical methods with experiment.

	Energy (eV)						
	This work			Theory			
State	Model 1	Model 2	Model 3	CASPT2[a]	MRDCI[b]	SAC-CI[c]	Experiment[d]
$^3B_2$	3.68	3.66		3.99	3.93	4.39	3.99
$^3A_1$	5.12		5.10	5.15	5.28	5.63	5.15
$^1B_2$	7.72	7.20		6.04	6.88	6.40	6.04
$^1A_1$	8.39		8.36	6.16	6.63	6.79	

[a]Reference [47].
[b]Reference [48].
[c]Reference [49].
[d]Experimental data were taken from Refs. [47,48,50–52] and references therein.

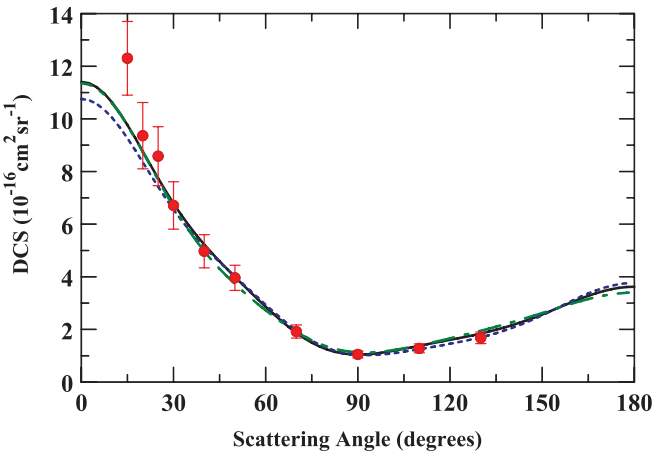

FIG. 3. (Color online) Differential cross sections for elastic electron scattering from furan at the E_0 value of 5.0 eV. Shown are the measurements of Khakoo *et al.* [23] and theoretical predictions from the three models considered in this study, called model 1 (black solid curve), model 2 (blue dashed curve), and model 3 (green dash-dotted curve).

described according to model 2, and the $^1A_1 \rightarrow {}^3A_1$ transition is described according to model 3. It is worth noting that, again, all states included in the space of coupled channels in model 2 (model 3) compete with the $^3B_2$ ($^3A_1$) state and with each other for the flux that defines the cross sections. The steps in determining the active space of coupled states were the same as described above, except for the fact that in model 2 the particle orbital subspace is composed of two orbitals of the b_1 type (a singlet and a triplet IVO out of the a_2 occupied orbital) and two IVOs of the a_2 type (a singlet and a triplet IVO out of the b_1 occupied orbital), while in model 3 it was composed of two orbitals of the b_1 type (a singlet and a triplet IVO out of the b_1 occupied orbital) and two IVOs of the a_2 type (a singlet and a triplet IVO out of the a_2 occupied orbital). As can be seen from Table II, the energy values for the $^3B_2$ and $^3A_1$ excited states obtained by means of the MOB-SCI strategy (models 1–3) are in very good agreement with the experimental data and also with theoretical results from more sophisticated electronic structure calculations. On the other hand, the excitation energies related to transitions from the ground state to the two singlet counterpart excited states, $^1B_2$ and $^1A_1$, were consistently higher (by more than 1 eV until around 2.2 eV) if compared to other data available in the literature. Here, it is important to recall that the small SCI calculation was carried out to provide an accurate description of the first few low-lying excited states of furan. Higher excited states obtained within the scope of the MOB-SCI strategy should therefore be regarded as pseudostates (i.e., states without an actual physical meaning), and for this reason they were not associated with any specific spectroscopy assignment.

In order to account for the polarization of the target we have adopted the following procedure: by freezing the occupied orbitals and the active particle orbitals described above, we have diagonalized a +2 cationic Fock operator where two electrons are subtracted from the a_2 occupied orbital and generated modified virtual orbitals (MVOs) [54] from the remaining virtual orbitals. We then considered single excitations from all valence occupied orbitals to the MVOs

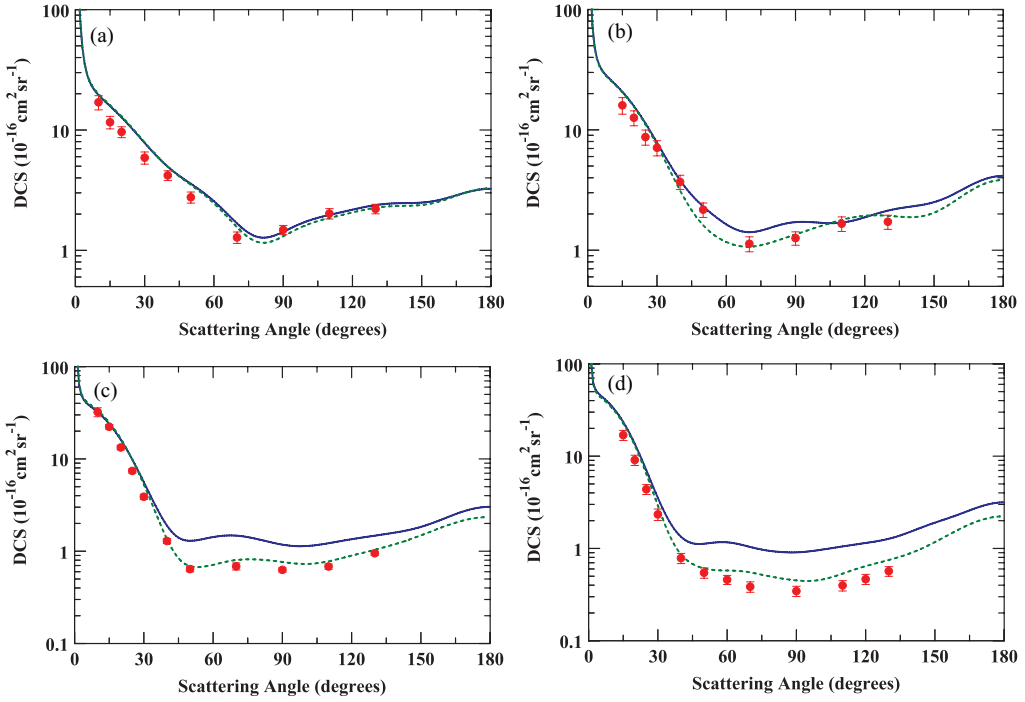

FIG. 4. (Color online) Differential cross section for elastic electron scattering from furan at E_0 values of (a) 7 eV, (b) 10 eV, (c) 20 eV, and (d) 30 eV. Shown are the measurements of Khakoo *et al.* [23] (solid red circles) and theoretical results from the present Schwinger multichannel calculations at the static-exchange–plus–polarization level (blue solid curve) and with the addition of multichannel coupling effects (green dashed curve).

with energies less than 10 hartrees as a cutoff criterion for the selection of the particle orbital space. The same set of MVOs was then used as scattering orbitals. We included singlet and triplet excitations, which resulted in a total of 19 230 doublet CSFs divided per symmetry as 5052 for A_1, 4581 for B_1, 5037 for B_2, and 4560 for A_2 for model 1; a total of 18 531 doublet CSFs divided per symmetry as 4878 for A_1, 4391 for B_1, 4879 for B_2, and 4383 for A_2 for model 2; and a total of 19 230 doublet CSFs divided per symmetry as 5064 for A_1, 4593 for B_1, 5025 for B_2, and 4548 for A_2 for model 3. Here it is important to mention that, although in all models we have used the same strategy for the treatment of polarization effects, the configuration state space obtained with the usual procedure is slightly different from one model to another. This difference occurs because the space of active states used to generate the CI-singles representation of the excited states of the target is different in each model. However, it is important to note that in all cases polarization effects were included in such a way to locate the resonances that appear in the elastic channel at the positions assigned as matching those observed in the literature (see, for instance, Refs. [21,23,24]). This aspect is important for theoretical models which involve electronic transitions to excited states for which the threshold is located at energies close to the position of resonances appearing in the elastic channel, as is the case for the $^3B_2$ and $^3A_1$ states of the furan molecule. A more detailed discussion on this subject can be found in Refs. [12,13].

Using this procedure, we obtained three models that, with respect to the orbital basis set and the description of polarization effects, are essentially equivalent. So, in principle, any discrepancy observed between the results obtained from different models reflects the fact that the multichannel coupling effects were included in a different way. That is, although the scattering calculations for our three models were performed with the same number of coupled channels (nine-state close-coupling level of approximation), the "type" of excited states and, as a consequence, the position of the excitation thresholds are found to be different in each case. Also important to the discussion carried out below is the fact that the potential describing the electron-molecule interaction changes to the extent that each one of the excited states belonging to the coupled-channel space is included in the scattering calculations. In fact, as can be seen below, the cross sections are so sensitive to the proximity of an excitation threshold that we observe sharp variations in the magnitude [for integral cross sections (ICSs)] and in shape (for DCSs) of the curves in the region around the energy corresponding to the opening of a given coupled channel.

VI. RESULTS AND DISCUSSION

Taking all these considerations in mind, in the next section we compare the data obtained from the three models described above with measurements taken earlier by our group [23].

A. Elastic scattering

The first results discussed are the DCSs for the elastic scattering at several representative E_0 values, shown in Figs. 3 and 4. We note here that although the scattering calculations have been carried out to generate electronically inelastic cross sections for the $^1A_1 \rightarrow {}^3B_2$ and the $^1A_1 \rightarrow {}^3A_1$ transitions, the elastic contribution to the scattering amplitudes is also simultaneously computed since the elastic channel is included

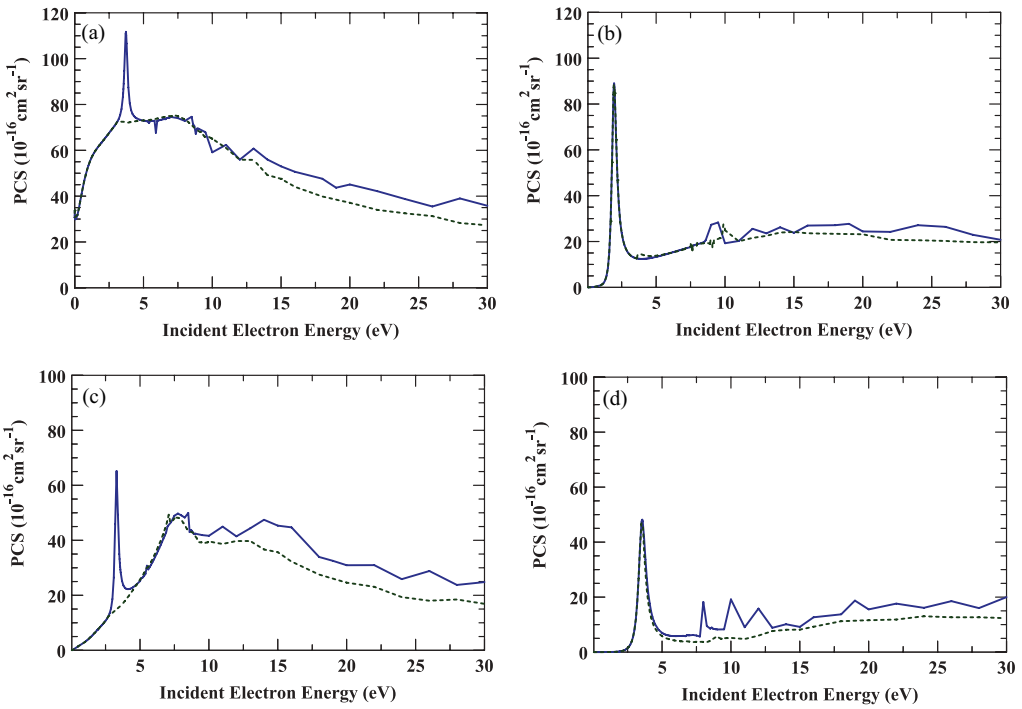

FIG. 5. (Color online) Comparisons between integral cross sections for elastic electron scattering from furan determined by models without (blue solid curve) and with (green dashed curve) multichannel coupling. The molecular symmetries shown are (a) A_1, (b) B_1, (c) B_2, and (d) A_2. See text for discussion.

TABLE III. Measured DCS and ICS data for excitation from the ground state to the $^3B_2$ state of furan by electron impact in units of 10^{-18} cm^2 sr^{-1} (DCS) and 10^{-18} cm^2 (ICS). The absolute uncertainties are shown in parentheses.

Scattering angle	5 eV	6 eV	7.5 eV	10 eV	15 eV
10°			0.49 (0.21)	0.79 (0.15)	0.36 (0.07)
15°			1.66 (0.30)		0.40 (0.09)
20°		0.89 (0.19)	2.40 (0.40)	1.49 (0.28)	0.47 (0.09)
25°		1.29 (0.23)	1.65 (0.34)		0.44 (0.08)
30°		1.88 (0.36)	2.22 (0.37)	1.39 (0.28)	0.53 (0.10)
35°	0.38 (0.22)	2.53 (0.40)			0.67 (0.11)
40°	0.74 (0.24)	2.66 (0.46)	3.18 (0.52)	1.73 (0.27)	0.69 (0.12)
50°	1.15 (0.22)	3.00 (0.49)	3.56 (0.59)	1.72 (0.29)	0.79 (0.15)
60°	1.47 (0.22)	3.46 (0.53)	3.53 (0.58)	1.99 (0.32)	0.79 (0.14)
70°				2.03 (0.32)	0.67 (0.11)
80°	1.81 (0.30)	5.18 (0.87)	5.59 (0.95)		0.68 (0.12)
90°	1.83 (0.26)	5.03 (0.80)	6.39 (1.07)	2.32 (0.31)	0.63 (0.12)
105°	1.93 (0.32)	4.49 (0.72)	6.75 (1.13)	2.37 (0.39)	0.77 (0.14)
120°	1.96 (0.34)	4.52 (0.71)	5.81 (0.95)	2.94 (0.49)	0.87 (0.15)
130°	2.02 (0.32)	4.91 (0.87)	5.88 (0.99)	3.54 (0.51)	1.10 (0.18)
ICS	20.2 (6.90)	52.4 (15.7)	63.8 (15.0)	31.4 (6.70)	11.0 (2.1)

in the space of coupled states. The results presented in Fig. 3 show that the DCSs obtained using model 1, model 2, and model 3 are, barring some minor differences, very consistent with each other and also in very good agreement with the experimental data from Ref. [23]. The same level of agreement between all three models considered in our study is observed for other energies in the range 0–30 eV (not shown here). These results show that the multichannel calculations carried out according to all the models used here provide elastic cross sections in very good agreement with the experiment. In Fig. 4 we present a comparison for the elastic cross sections obtained in model 1 calculations performed at the static-exchange–plus–polarization (SEP) level of approximation with and without inclusion of channel coupling. The importance of including multichannel effects for the description of the elastic scattering at high energies is clearly highlighted by the improved agreement with experiment at 20 and 30 eV. At those energies the elastic DCSs are lowered due to the flux leakage to the now-open inelastic channels. This effect has also been obtained by using complex (absorption) potentials [55]. In order to give an indication of the net influence of channel-coupling effects on the elastic results, Fig. 5 shows a symmetry decomposition of the elastic ICS, with and without channel coupling. For all molecular symmetries shown, the ICS calculated under the single-channel model shows pseudoresonances about the threshold energies of the excited states. In the multichannel calculation these states are kept open, and the opening state can compete with the elastic for cross-section flux. In the single-channel calculation where they are kept closed, the absence of this competition results in spurious spikes in the ICS.

B. Electronic excitation

The measured DCSs tabulated for the excitation of all states experimentally investigated and included in the unfolding analysis are shown in Table III ($^3B_2$) and Table IV ($^3A_1$), along with the corresponding ICSs. Theory for the triplet states is limited in energy range to $E_0 \leqslant 10$ eV due to the growing number of open channels with increasing E_0 values. Both measured and calculated DCSs of this work are shown for comparison in Fig. 6 for all E_0 values for the excitation of the $^3B_2$ state from the ground state and in Fig. 7 for the excitation of the $^3A_1$ state. The quantitative agreement between the experiment and theory is reasonable, considering the complexity of the problem, at the lower E_0 values of 5, 6, and 7.5 eV. However, none of the calculations reproduce the rapid drop in forward scattering observed in the experimental DCSs at these energies in the region of small θ for both states. At an energy of 10 eV the discrepancy among theoretical

TABLE IV. Measured DCS and ICS data for excitation from the ground state to the $^3A_1$ state of furan by electron impact in units of 10^{-18} cm^2 sr^{-1} (DCS) and 10^{-18} cm^2 (ICS). The absolute uncertainties are shown in parentheses.

Scattering angle	7.5 eV	10 eV	15 eV
10°		0.83 (0.12)	0.88 (0.14)
15°	3.30 (0.52)		0.76 (0.12)
20°	5.60 (0.77)	1.53 (0.22)	0.86 (0.17)
25°	1.93 (0.46)		0.76 (0.12)
30°	2.62 (0.44)	1.13 (0.20)	0.73 (0.12)
35°			0.97 (0.16)
40°	3.41 (0.56)	1.49 (0.20)	0.92 (0.16)
50°	3.59 (0.60)	1.68 (0.23)	0.91 (0.18)
60°	4.40 (0.70)	2.01 (0.30)	0.93 (0.16)
70°			0.73 (0.13)
80°	7.11 (1.18)	2.19 (0.33)	0.69 (0.12)
90°	8.72 (1.38)	1.96 (0.25)	0.71 (0.12)
105°	8.84 (1.41)	2.24 (0.34)	0.70 (0.15)
120°	7.39 (1.15)	2.38 (0.36)	0.93 (0.16)
130°	7.00 (1.16)	2.75 (0.37)	1.32 (0.21)
ICS	78.7 (13.0)	27.3 (4.10)	12.8 (2.70)

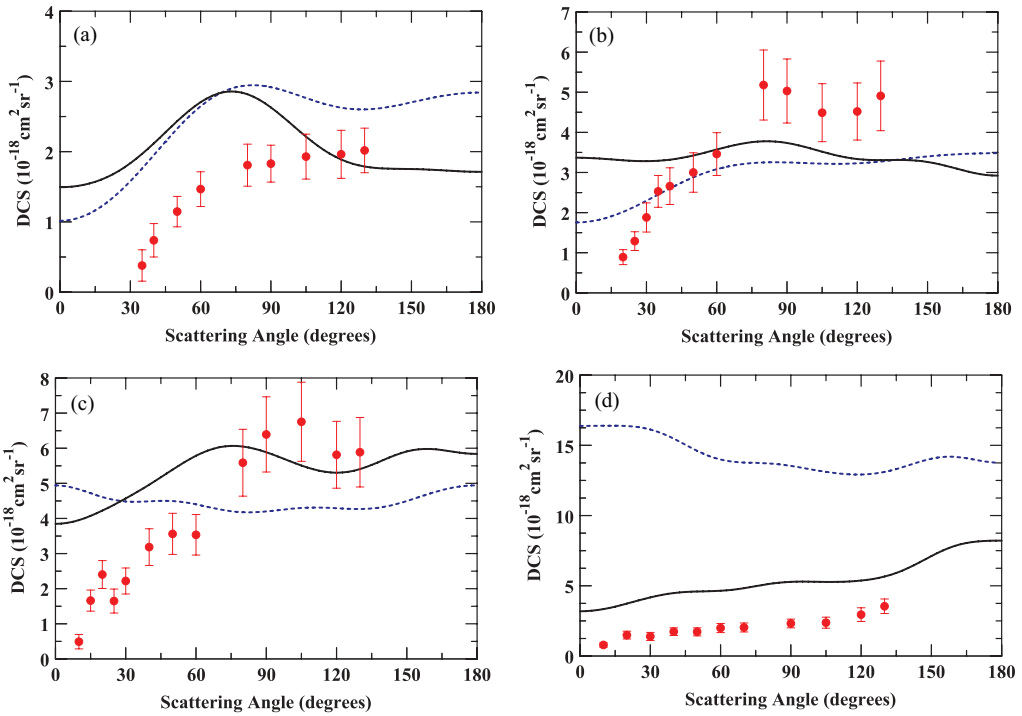

FIG. 6. (Color online) Differential cross section for the electronic excitation from ground state to the $^3B_2$ state of furan by electron impact at an energy of (a) 5 eV, (b) 6 eV, (c) 7.5 eV, and (d) 10 eV. The present experimental data (solid circles) are shown, as well as the present theoretical results from model 1 (black solid curve) and model 2 (blue dashed curve).

and experimental results is about a factor of 3, even though, in the case of the $^3B_2$ state, the shape of the DCS curve is similar. The model 1 DCSs show significantly better agreement with the experimental data for 10 eV than the others. The backward profile of the DCSs suggests that the excitation of these features is typical of that found in spin-exchange-type scattering, i.e., a singlet $\longleftrightarrow$ triplet excitation which is similar for both excitations.

ICS results for the study of the electronic excitation of furan by electron impact obtained from models 1–3 are shown in Figs. 8 and 9 for the excitation of the $^3B_2$ state and the $^3A_1$ state, respectively. Our calculated ICS curves display the presence of several structures, some of which are related to the opening of states that belongs to the space of coupled channels included in the multistate calculations employed. The threshold energies for these states are indicated by the arrows in Figs. 8 and 9, where near these thresholds we observe sharp variations in the magnitude of the ICSs. Other structures appearing at different energies may be related to core-excited shape resonances or may also be spurious; a careful investigation into these features is needed before any assignments are made. Encouragingly, both theoretical results and experimental results show both compatible magnitudes and similar trends in the dependency of the integral cross section with the energy, at least at incident energies less than 10 eV. At the higher energy of 10 eV agreement is not as good, with a difference of a factor of about 3.

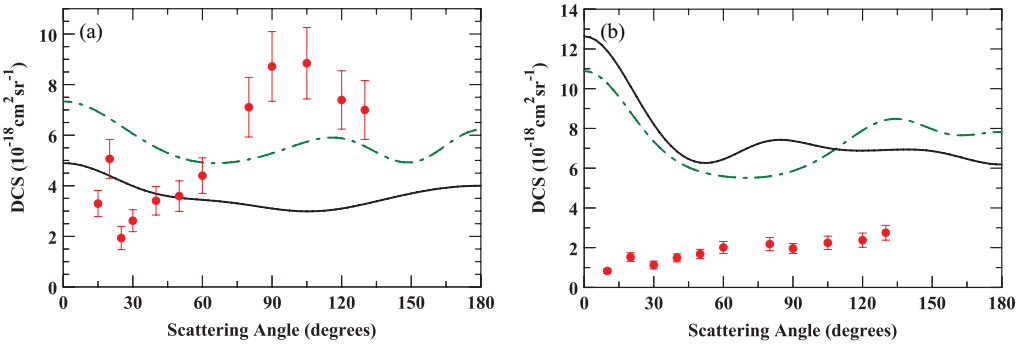

FIG. 7. (Color online) Differential cross section for the electronic excitation from ground state to the $^3A_1$ state of furan by electron impact at incident energies of (a) 7.5 eV and (b) 10 eV. The present experimental data points (red circles) are shown, as well as the present theoretical results from model 1 (black solid curve) and model 3 (green dash-dotted curve).

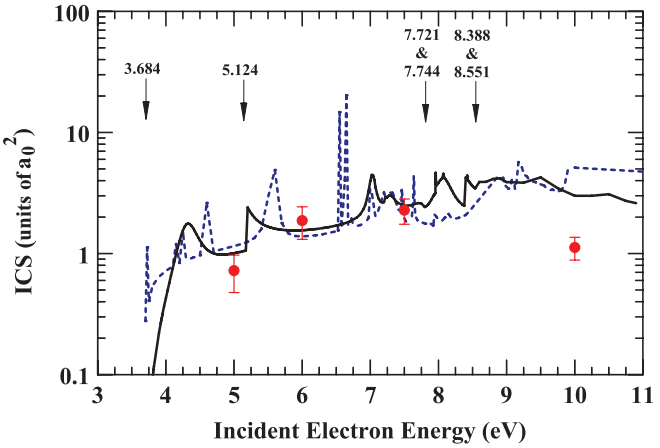

FIG. 8. (Color online) Integral cross section for the electronic excitation from ground state to the $^3B_2$ state of furan by electron impact. Shown are the present experimental data (solid red circles) and theoretical results from model 1 (black solid curve) and model 2 (blue dashed curve).The arrows indicate the energy thresholds of the states included in the space of coupled channels as listed in the first row of Table I.

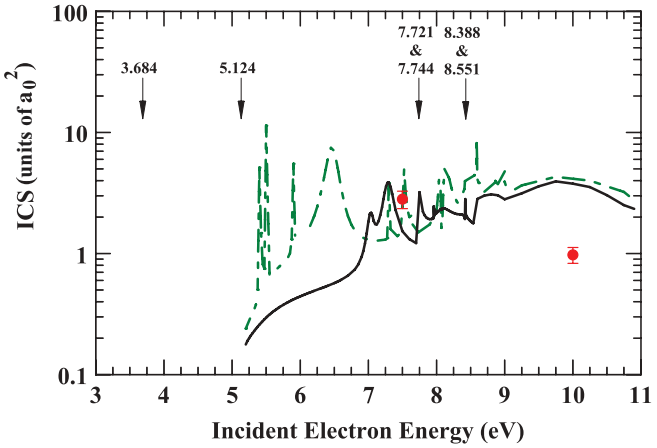

FIG. 9. (Color online) Integral cross section for the electronic excitation from ground state to the $^3A_1$ state of furan by electron impact. Shown are the present experimental data (solid red circles) and theoretical results from model 1 (black solid curve) and model 3 (green dash-dotted curve). The arrows indicate the energy thresholds of the states included in the space of coupled channels as listed in the first row of Table I.

VII. CONCLUSIONS

In this work, we presented experimental and theoretical results for the excitation of the two lowest triplet states of furan by electron impact. Furan was chosen because it represents a system simpler than, but similar to, the 2-deoxyribose molecule, the sugarlike component of the DNA backbone, and because it presents two prominent shape resonances around the excitation threshold of the $^3B_2$ state. After performing a series of tests to evaluate the numerical stability of our scattering calculations and also to increase the grid resolution of the energy points, we concluded that model 1 provides ICSs and DCSs which show better agreement overall with the experiment compared to the other two models. Finally, we would like to call attention to the fact that the DNA nitrogenated bases, as well as many other organic molecules of biological or technological relevance, have excited states in the energy range from 3 to 5 eV. As a consequence, an adequate description of electron-impact electronic excitation to such low-lying states must necessarily be carried out including polarization effects of the target in order to provide reliable cross-section values. In terms of experimental effort, it is important to continue such investigations at near-threshold energies, where it becomes possible for meaningful close-coupling multistate models to work, and to provide further tests for experiment before both experiments and models can be extended to higher energies.

ACKNOWLEDGMENTS

This work was funded through a collaborative program by the U.S. National Science Foundation under Grants No. PHY 0653452 and No. PHY 0653396 and by the Brazilian agency Conselho Nacional de Desenvolvimento Científico e Tecnológico (CNPq) under Project No. 490415/2007-5. R.F.d.C., M.H.F.B., M.C.A.L. and M.A.P.L. acknowledge additional support from CNPq and from the Brazilian agencies Coordenação de Aperfeiçoamento de Pessoal de Nível Superior (CAPES), Fundação de Amparo à Pesquisa do Estado de São Paulo (FAPESP), the Paraná state agency Fundação Araucária, Fundação de Amparo à Pesquisa do Estado de Minas Gerais (FAPEMIG), and Financiadora de Estudos e Projetos (FINEP) under Project No. CT-Infra 1. M.H.F.B. further acknowledges computational support from Professor Carlos M. de Carvalho at DF-UFPR. Computational support from Centro de Computação John David Rogers (CCJDR) and from Centro Nacional de Processamento de Alto Desempenho em São Paulo (CENAPAD), where the calculations in Brazil were performed, is gratefully acknowledged.

[1] B. Boudaïffa, P. Cloutier, D. Hunting, M. A. Huels, and L. Sanche, Science **287**, 1658 (2000).
[2] X. Pan, P. Cloutier, D. Hunting, and L. Sanche, Phys. Rev. Lett. **90**, 208102 (2003).
[3] M. A. Huels, B. Boudaïffa, P. Cloutier, D. Hunting, and L. Sanche, J. Am. Chem. Soc. **125**, 4467 (2003).
[4] F. Martin, P. D. Burrow, Z. Cai, P. Cloutier, D. Hunting, and L. Sanche, Phys. Rev. Lett. **93**, 068101 (2004).
[5] L. Sanche, Eur. Phys. J. D **35**, 367 (2005).
[6] P. L. Levesque, M. Michaud, W. Cho, and L. Sanche, J. Chem. Phys. **122**, 224704 (2005).
[7] F. A. Gianturco, F. Sebastianelli, R. R. Lucchese, I. Baccarelli, and N. Sanna, J. Chem. Phys. **128**, 174302 (2008).
[8] C. Winstead and V. McKoy, J. Chem. Phys. **125**, 174304 (2006).
[9] A. Dora, J. Tennyson, L. Bryjko, and T. van Mourik, J. Chem. Phys. **130**, 164307 (2009).

[10] M. Bazin, M. Michaud, and L. Sanche, J. Chem. Phys. **133**, 155104 (2010).
[11] M. Michaud, M. Bazin, and L. Sanche, Int. J. Radiat. Biol. **88**, 15 (2012).
[12] R. F. da Costa, M. H. F. Bettega, and M. A. P. Lima, Phys. Rev. A **77**, 012717 (2008).
[13] R. F. da Costa, M. H. F. Bettega, and M. A. P. Lima, Phys. Rev. A **77**, 042723 (2008).
[14] M. Allan, C. Winstead, and V. McKoy, Phys. Rev. A **77**, 042715 (2008).
[15] See, for instance, T. Fleig, S. Knecht, and C. Hättig, J. Phys. Chem. A **111**, 5482 (2007), and references therein.
[16] C. S. Trevisan, A. E. Orel, and T. N. Rescigno, Phys. Rev. A **70**, 012704 (2004); C. Winstead and V. McKoy, Phys. Rev. Lett. **98**, 113201 (2007); E. M. de Oliveira, M. A. P. Lima, M. H. F. Bettega, S. d'A. Sanchez, R. F. da Costa, and M. T. do N. Varella, J. Chem. Phys. **132**, 204301 (2010); Z. Masin and J. D. Gorfinkiel, *ibid.* **135**, 144308 (2011), and references therein.
[17] E. H. van Veen, Chem. Phys. Lett. **41**, 535 (1976).
[18] W. M. Flicker, O. A. Mosher, and A. Kuppermann, Chem. Phys. Lett. **38**, 489 (1976).
[19] W. M. Flicker, O. A. Mosher, and A. Kuppermann, J. Chem. Phys. **64**, 1315 (1976).
[20] M. V. Muftakhov, N. L. Asfandiarov, and V. I. Khvostenko, J. Electron Spectrosc. Relat. Phenom. **69**, 165 (1994); V. I. Khvostenko, A. S. Vorobyov, and O. G. Khvostenko, J. Phys. B **23**, 1975 (1990).
[21] A. Modelli and P. W. Burrow, J. Phys. Chem. A **108**, 5721 (2004).
[22] M. H. F. Bettega and M. A. P. Lima, J. Chem. Phys. **126**, 194317 (2007).
[23] M. A. Khakoo, J. Muse, K. Ralphs, R. F. da Costa, M. H. F. Bettega, and M. A. P. Lima, Phys. Rev. A **81**, 062716 (2010).
[24] C. Szmytkowski, P. Możejko, E. Ptasinska-Denga, and A. Sabisz, Phys. Rev. A **82**, 032701 (2010).
[25] P. Sulzer *et al*., J. Chem. Phys. **125**, 044304 (2006).
[26] F. Motte-Tollet, G. Eustatiu, and D. Roy, J. Chem. Phys. **105**, 7448 (1996).
[27] M. Dampc and M. Zubek, Int. J. Mass Spectrom. **277**, 52 (2008).
[28] L. R. Hargreaves, R. Albaridy, G. Serna, M. C. A. Lopes, and M. A. Khakoo, Phys. Rev. A **84**, 062705 (2011).
[29] K. Takatsuka and V. McKoy, Phys. Rev. A **24**, 2473 (1981); **30**, 1734 (1984).
[30] M. H. F. Bettega, L. G. Ferreira, and M. A. P. Lima, Phys. Rev. A **47**, 1111 (1993).
[31] M. A. Khakoo, C. E. Beckmann, S. Trajmar, and G. Csanak, J. Phys. B **27**, 3159 (1994).
[32] J. H. Brunt, G. C. King, and F. H. Read, J. Phys. B **10**, 1289 (1977).
[33] M. A. Khakoo, H. Silva, J. Muse, M. C. A. Lopes, C. Winstead, and V. McKoy, Phys. Rev. A **78**, 052710 (2008).
[34] M. Hughes, K. E. James Jr., J. G. Childers, and M. A. Khakoo, Meas. Sci. Technol. **14**, 841 (1994).
[35] L. R. Le Clair and S. Trajmar, J. Phys. B **29**, 5543 (1996).
[36] D. V. Fursa and I. Bray, Phys. Rev. A **52**, 1279 (1995).
[37] E. Schow, K. Hazlett, J. G. Childers, C. Medina, G. Vitug, I. Bray, D. V. Fursa, and M. A. Khakoo, Phys. Rev. A **72**, 062717 (2005).
[38] A. Guiliani and M. J. Hubin-Franskin, Int. J. Mass Spectrom. **205**, 163 (2001).
[39] QTIPLOT, [http://www.soft.proindependent.com/qtiplot.html].
[40] R. F. da Costa, F. J. da Paixão, and M. A. P. Lima, J. Phys. B **37**, L129 (2004); **38**, 4363 (2005).
[41] G. B. Bachelet, D. R. Hamann, and M. Schlüter, Phys. Rev. B **26**, 4199 (1982).
[42] P. Chaudhuri, M. T. do N. Varella, C. R. C. Carvalho, and M. A. P. Lima, Nucl. Instrum. Methods Phys. Res., Sect. B **221**, 69 (2004); Phys. Rev. A **69**, 042703 (2004).
[43] *CRC Handbook of Chemistry and Physics*, 79th ed., edited by D. R. Lide (CRC, Boca Raton, FL, 1998).
[44] M. H. F. Bettega, A. P. P. Natalense, M. A. P. Lima, and L. G. Ferreira, Int. J. Quantum Chem. **60**, 821 (1996).
[45] T. H. Dunning Jr., J. Chem. Phys. **53**, 2823 (1970).
[46] W. J. Hunt and W. A. Goddard, Chem. Phys. Lett. **3**, 414 (1969).
[47] H. Nakatsuji, O. Kitao, and T. Yonezawa, J. Chem. Phys. **83**, 723 (1985).
[48] L. Serrano-Andres, M. Merchan, I. Nebot-Gil, B. O. Roos, and M. Fulscher, J. Am. Chem. Soc. **115**, 6184 (1993).
[49] J. Wan, J. Meller, M. Hada, M. Ehara, and H. Nakatsujia, J. Chem. Phys. **113**, 7853 (2001).
[50] M. H. Palmer, I. C. Walker, C. C. Ballard, and M. F. Guest, Chem. Phys. **192**, 111 (1995).
[51] M. H. Palmer, I. C. Walker, and M. F. Guest, Chem. Phys. **238**, 179 (1998).
[52] H. Nakano, T. Tsuneda, T. Hashimoto, and K. Hirao, J. Chem. Phys. **104**, 2312 (1996).
[53] A. Kokalj, J. Mol. Graphics Modell. **17**, 176 (1999).
[54] C. W. Bauschlicher, J. Chem. Phys. **72**, 880 (1980).
[55] E. A. y Castro, G. L. C. de Souza, I. Iga, L. E. Machado, L. M. Brescansin, and M.-T. Lee, J. Electron Spectrosc. Relat. Phenom. **159**, 30 (2007).